coatings

MDPI

Article

Prediction of Microstructure and Mechanical Properties of Atmospheric Plasma-Sprayed 8YSZ Thermal Barrier Coatings Using Hybrid Machine Learning Approaches

Han Zhu [1,2,3], Dongpeng Li [4], Min Yang [4] and Dongdong Ye [5,6,7,8,*]

1 Shi-Changxu Innovation Center for Advanced Materials, Institute of Metal Research, Chinese Academy of Sciences, Shenyang 110016, China
2 School of Materials Science and Engineering, Northeastern University, Wenhua Road, Shenyang 110819, China
3 China Coal Xinji Lixin Power Generation Co., Ltd., Bozhou 236000, China
4 School of Mechanical and Power Engineering, East China University of Science and Technology, Shanghai 200237, China
5 School of Artificial Intelligence, Anhui Polytechnic University, Wuhu 241000, China
6 Anhui Polytechnic University Asset Management Co., Ltd., Wuhu 241000, China
7 Anhui Key Laboratory of Mine Intelligent Equipment and Technology, Anhui University of Science & Technology, Huainan 232001, China
8 Anhui Key Laboratory of Detection Technology and Energy Saving Devices, Anhui Polytechnic University, Wuhu 241000, China
* Correspondence: ddyecust@ahpu.edu.cn

Abstract: The preparation of thermal barrier coatings (TBCs) is a complex process involving the integration of physics and chemistry, mainly involving the flight behavior and deposition behavior of molten particles. The service life and performance of the TBCs were determined by various factors, especially the preparation process parameters. In this work, to set up the quantitative characterization model between the preparation process parameters and the performance characteristic parameters, the ceramic powder particle size, spraying power and spraying distance were treated as the model input parameters, the characteristic parameters of microstructure properties represented by the porosity, circularity and Feret's diameter and the mechanical property represented by the interfacial binding strength and macrohardness were treated as the model output. The typical back propagation (BP) model and extreme learning machine (ELM) model combined with flower pollination algorithm (FPA) optimization algorithm were employed for modeling analysis. To ensure the robustness of the obtained regression prediction model, the k-fold cross-validation method was employed to evaluate and analyze the regression prediction models. The results showed that the regression coefficient *R* value of the proposed FPA-ELM hybrid machine learning model was more than 0.94, the root-mean-square error (RMSE) was lower than 2 and showed better prediction accuracy and robustness. Finally, this work provided a novel method to optimize the TBCs preparation process, and was expected to improve the efficiency of TBCs preparation and characterization in the future.

Keywords: thermal barrier coatings; machine learning; k-fold cross-validation; FPA-ELM

Citation: Zhu, H.; Li, D.; Yang, M.; Ye, D. Prediction of Microstructure and Mechanical Properties of Atmospheric Plasma-Sprayed 8YSZ Thermal Barrier Coatings Using Hybrid Machine Learning Approaches. *Coatings* **2023**, *13*, 602. https://doi.org/10.3390/coatings13030602

Academic Editor: Cecilia Bartuli

Received: 21 February 2023
Revised: 4 March 2023
Accepted: 8 March 2023
Published: 12 March 2023

1. Introduction

The gas turbine engine is a power machine that drives the impeller to rotate at high speeds with the energy of a flowing working medium. It is widely used in the power engine of civil aviation and military aircraft, ship power and vehicles. The thermal efficiency of gas turbine has been greatly improved from year to year [1,2]. However, high efficiency, energy-saving and environmental protection gas turbine has been the goal of new generation aero-engine. Further improving the thrust-weight ratio and thermal efficiency of gas turbines has become a core issue. Nevertheless, the increase of the thermal efficiency of gas turbine will inevitably greatly raise the working temperature of the combustion chamber,

which poses a new challenge to the maximum service temperature of high-temperature components of gas turbine [3–5].

Thermal barrier coatings are generally composed of the ceramic layer with high temperature resistance, low thermal conductivity and corrosion resistance, as well as the metal bonding layer with transition performance. It is widely employed to significantly reduce the surface temperature of hot-section components, improve the resistance of matrix alloys to high temperature oxidation corrosion, prolong the working life of the blades, and promote the thrust and efficiency of the aero-engine [6,7].

A higher inlet temperature results in higher requirements for the service temperature of superalloys and the performance of thermal barrier coatings. Plenty of research has been carried out in developing new superalloy materials and thermal barrier coatings materials, improving the TBCs structure and preparation methods [8,9]. At present, plasma spraying is still treated as the most common TBCs preparation method. According to the atmospheric plasma spraying, plasma arc was employed to heat the coatings powder so as to enter the molten or semi-molten powder droplets. Then, the droplets are sprayed out at a high speed with the air flow through the spray gun, and then impinged on the metal substrate, deposited on the substrate surface, rapidly cooled, solidified and shrunken on the substrate surface. It forms a mechanical inlay with the surface of the base material, which is stacked layer by layer, and finally forms the thermal barrier coatings. Among the spraying processes, the study of improving the microstructure of thermal barrier coatings has been widely concerned. It is expected that by optimizing the spraying process, the thermal barrier coatings with excellent performance can be prepared, so as to extend the service life of thermal barrier coatings [10–15].

Taking atmospheric plasma spraying as an example, in the process of coating preparation, there are many factors affecting the TBCs microstructure and mechanical properties. The TBCs quality is not only affected by the TBCs material itself, but also depends on the spraying process to a large extent. Plenty of researchers have conducted a large number of studies on the relationship between TBCs service performance and spraying process parameters, and obtained plenty of beneficial results [16–18]. However, there are dozens of spraying process parameters in the actual spraying process, and various process parameters will form mutual coupling. Therefore, the relationship between TBCs microstructure and spraying process parameters is still not fully understood. It is of great significance to establish the relationship between spraying process and TBCs microstructure properties and explore the influence of spraying process parameters on TBCs properties to improve the preparation stability. However, it is impossible to explore all spraying parameters at the same time [19,20]. Based on this problem, in this work, as shown in Figure 1, the research was carried out to explore the quantitative relationship between process parameters, microstructure characteristics and mechanical properties, and to model and analyze the complex nonlinear relationship by combining machine learning and big data technology, so as to further provide scientific guidance for the TBCs preparation. The main research content of this paper was to use spraying process parameters as input, microstructure and mechanical properties as output, combined with machine learning (ML) and optimization algorithm for modeling, and then a cross-validation was applied to evaluate the modeling results. More details will be shown in the following sections.

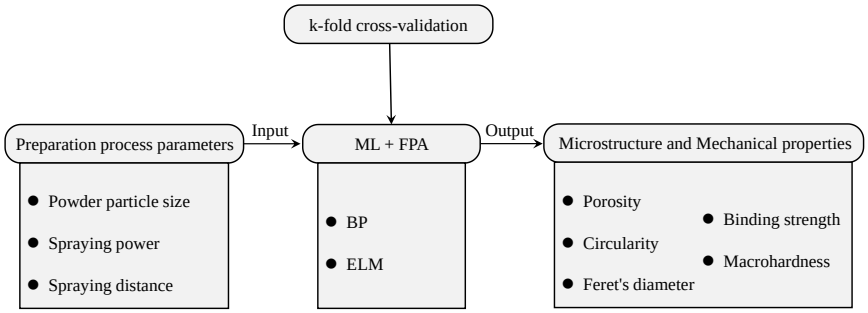

Figure 1. Research content structure diagram.

2. Experiment and Modeling

2.1. YSZ TBCs Preparation and Characterization

2.1.1. Coatings Preparation

Gas turbine blades were usually used in harsh environments with high temperature and high pressure, and their working conditions were very harsh, so strict requirements were put forward for blade materials. Since nickel/cobalt superalloys were often employed in gas turbine blades, Inconel600 nickel-based superalloy was employed as the substrate material in this experiment. The thermal barrier coatings materials used in the experiment contained metal bonding layer material and surface ceramic layer material. The metal bonding layer material used in the experiment was NiCoCrAlY anti-high temperature oxidation alloy powder, which could effectively improve the physical compatibility between the ceramic layer and the base metal and the mismatch of thermal expansion coefficient and other problems. A disc-shaped Inconel600 with a thickness of 3 mm and a diameter of 25.4 mm was used as the matrix material for the TBCs sample. The substrate surface was roughened by sand blasting and ultrasonic cleaned by acetone. The adhesive layer and YSZ ceramic coating were deposited on the substrate by atmospheric plasma spraying. The adhesive layer uses NiCrAlY powder with particle sizes of 45–106 μm. Two kinds of 8YSZ (8 wt.%, Y_2O_3 stabilized ZrO_2, Beijing Sanspuri New Material Co., Ltd., Beijing, China) powders with particle sizes of 15–45 μm and 45–90 μm were used as raw materials for the preparation of ceramic coatings. The morphologies of the two YSZ powders were shown in Figure 2.

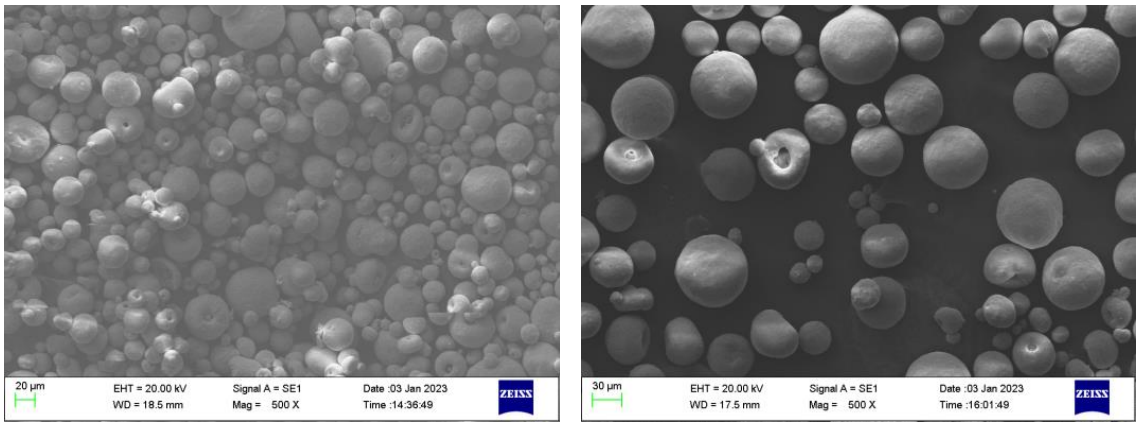

(**a**) (**b**)

Figure 2. SEM images showing morphologies of the 8YSZ powders: (**a**) 15–45 μm; (**b**) 45–90 μm.

2.1.2. Coatings Characterization

TBCs microstructure was extracted by scanning electron microscopy (SEM, ZEISS EVO MA15, Carl Zeiss SMT Ltd., Oberkochen, Germany), according to the ASTM E 2109 B standard, the image analysis software ImageJ Software (vl.46, National Institutes of Health,

Bethesda, MD, USA) was used to observe the metallographic sample of the coating, and different values were set on the micrograph of the coating by the grayscale of the photo. Then, according to the values of different sizes, the black region (the pore region) in the coating was calibrated. Finally, the porosity was estimated by the proportion of the black region. All types of pores were isolated for image segmentation through threshold segmentation and binarization. As shown in Figure 3, the black area represents the pores and the white area represents the YSZ coating. To further distinguish the spherical pores (mainly for all kinds of large pores and small pores) and crack network (mainly for the coating particles between the layer of uncombined areas and various cracks), open operation was employed to conduct the image processing. The so-called open operation was conducted through continuous corrosion, followed by the expansion operation. The corrosion filter removed pixels from the edges of an object, while the dilation filter added pixels to the edges of an object in a binary image, where the object was the adjacent black area of the binary image and the rest of the white area was the background. Obviously, it was far from sufficient to use porosity alone to characterize the microstructure characteristics of porous ceramic layer. Therefore, the circularity and Feret's diameter (the longest distance between any two points along the pore boundary) was added to further characterize the microstructure of the TBCs [21]. With the application of the ImageJ software with powerful statistical ability, for each spraying parameter, ten cross-section SEM images without overlapping were selected for the statistical analysis of the microstructure characteristics.

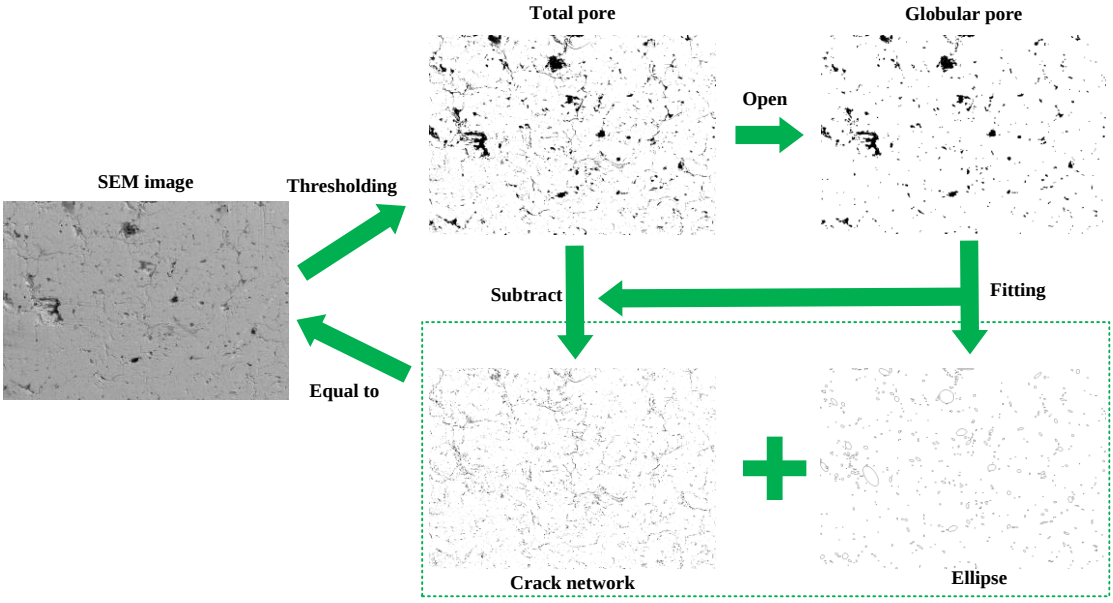

Figure 3. Extraction of microscopic features of thermal barrier coatings.

According to the ASTM C633–01 standard, the adhesion strength of TBCs was tested by the determination of adhesion of coats-pull-off test. The bonding test was to use E7 adhesive (Shanghai synthetic resin research institute) to combine the coated end face with a stainless steel column with the same size of sandblasted end face. The bonded samples were placed in an oven at 120 °C for heat preservation. The bonded sample was fixed on the mechanical property testing machine for tensile test, and the tensile speed was 2 mm/min. Five samples were tested in each group, and the average value of five samples was taken as the experimental result. Vickers indentation fracture test (VIF) was a common technique for evaluating the cracking resistance of brittle ceramic materials. According to the GB/T 37900–2019, Vickers hardness tester was applied to the cross section of the coating with a relatively high pressure mark load to force the coating to crack. The influence of spraying process parameters on the mechanical properties was investigated through a statistical

analysis of the TBCs crack behavior. The Vickers indentation method was used to measure the macroscopic hardness under the loading of 1000 g and a loading time of 15 s.

2.2. Hybrid Machine Learning Models

2.2.1. Back Propagation and Extreme Learning Machines Algorithms

There was a complex nonlinear mapping relationship between the spraying parameters and the physical and chemical properties of the coatings to be prepared. The quantitative relationship between the microstructure characteristics (porosity, circularity and Feret's diameter) and mechanical properties (interfacial binding strength and macrohardness) of the thermal barrier coatings need to be established, and machine learning was expected to provide a novel solution to this problem [22–25]. However, considering the prediction model construction problem of multi-parameter input and output, the machine learning model of a single input corresponding to a single output or multiple inputs corresponding to a single output would not be applicable. After comprehensive consideration, a neural network algorithm was proposed to solve this problem.

Artificial neural network (ANN), based on the bionics principle, abstracted the information conduction mechanism of human brain neurons from the perspective of information processing, so as to establish a widely interconnected computing network with generalization. Neural network not only had high computing power, but also had strong association ability and adaptability, which made it able to realize nonlinear mapping and able to carry out complex and tedious calculations. Its special nonlinear information processing ability also solved the defect of traditional artificial intelligence to intuition, so the neural network had been widely used in the field of pattern recognition and prediction. Generally, the most commonly used ANN algorithm was the BP neural network, which was composed of input layer, hidden layer and output layer. The hidden layer could be designed as single layer or multi-layer. Usually, the typical three-layer structure could take into account the complexity of the model and the workload during calculation, so this work adopted the three-layer structure. In view of the fact that this algorithm had been widely used in all kinds of nonlinear modeling prediction problems, there has been a lot of research conducted and available in the literature for reference, so there was no longer a need for an introduction [26,27].

As shown in Figure 4, extreme learning machine was a single hidden layer feedforward neural network. This model used random weights, thresholds and Moore–Penrose generalized inverse matrix theory to obtain the weight parameters of the output network and output the final results. According to the network architecture of extreme learning machine, compared with the traditional single-hidden layer feedforward neural network, the training process of this network was simple and the generalization ability was stronger [28,29]. Therefore, this study adopted BP algorithm and ELM algorithm to conduct modeling analysis. The implementation process of ELM algorithm was as follows:

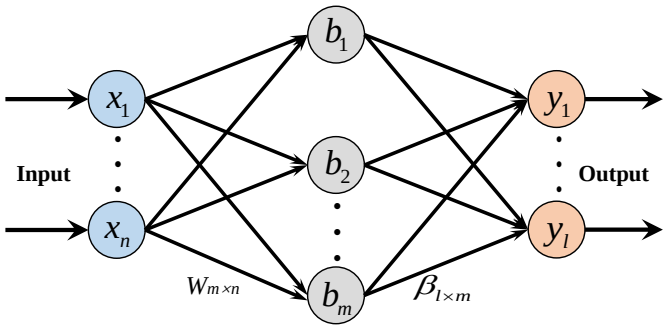

Figure 4. The architecture of the ELM model.

Given N samples $(x_j, t_j) \quad (j = 1, 2, \ldots, N)$, the extreme learning machine model with L hidden layer nodes was as follows:

$$\sum_{i=1}^{L} \beta_i g_i(x_j) = \sum_{i=1}^{L} \beta_i g(w_i x_j + b_i) = y_i, j = 1, 2, \ldots, N \tag{1}$$

where, w_i was the connection weight vector from the input layer to the hidden layer, b_i was the node threshold of the Z hidden layer, β_i was the connection weight vector from the hidden layer to the output layer. The goal of the single hidden layer neural network was to make the actual output infinitely close to the expected output t_j, which was as follows:

$$\sum_{i=1}^{L} \beta_i g(w_i x_j + b_i) = t_j, j = 1, 2, \ldots, N \tag{2}$$

The N equations it contained could be abbreviated as follows:

$$H\beta = T \tag{3}$$

where H was the output matrix of the hidden layer, β was the weight matrix of the output layer, and T was the target expected output matrix.

$$H = H(w_1, w_2, \ldots, w_L, b_1, b_2, \ldots, b_L, x_1, x_2, \ldots, x_N) == \begin{bmatrix} g(w_1 \cdot x_1 + b_1) & \cdots & g(w_L \cdot x_1 + b_1) \\ \vdots & \ldots & \vdots \\ g(w_1 \cdot x_N + b_1) & \cdots & g(w_L \cdot x_N + b_L) \end{bmatrix}_{N \times L} \tag{4}$$

$$\beta = \begin{bmatrix} \beta_1^T \\ \vdots \\ \beta_L^T \end{bmatrix}_{L \times m}, T = \begin{bmatrix} t_1^T \\ \vdots \\ t_L^T \end{bmatrix}_{N \times m} \tag{5}$$

In this ELM algorithm, the weight of the input layer and the hidden layer were biased random assignments, and the training of the ELM network could be converted into the least squares solution problem of solving the output weight β, where the calculation formula of the output weight β was as follows:

$$\beta = H^+ T \tag{6}$$

where H^+ was the generalized inverse matrix of H. When N samples were given, the extreme learning machine with L hidden layer nodes was established according to the following steps:

1. (a) Random assignment of input layer weight and hidden layer bias;
2. (b) Calculate the output matrix of hidden layer, H = g(WX + B);
3. (c) Calculate the output weight, $\beta = H^+ T$.

2.2.2. Flower Pollination Algorithm

Considering that the optimal network structure could not be automatically found in the modeling process of ELM network, the accuracy and stability of the model would be poor in the face of complex and irregular data. To enhance the stability and prediction accuracy of ELM network, after determining the optimal activation function of ELM and the number of hidden layer nodes, swarm intelligent optimization algorithm was used to optimize the connection weight and neuronal threshold in the ELM model to improve the accuracy and generalization ability of ELM prediction model.

Flower pollination algorithm (FPA) was a new meta-heuristic swarm intelligent optimization algorithm proposed by Yang Xin-She in 2012 [30]. This algorithm was inspired by the pollination process of the flowers of the natural flowering plants, and combined the

advantages of cuckoo optimization algorithm and bat algorithm. Yang used this algorithm to solve the multi-objective optimization problem in 2013, and achieved good results. Since the conversion probability parameter was used to realize the dynamic control of the conversion process between global search and local search, which better solved the balance problem between global search and local search, FPA was simple to implement with few parameters and was easy to adjust. Meanwhile, Levy flight mechanism was adopted to make it have good global optimization ability. Based on this, FPA was selected to optimize the BP and ELM models in this work.

The process of pollen pollination in nature was very complicated. When designing an algorithm by simulating the process of pollen pollination, it was difficult to completely simulate every detail of the process of pollen pollination. In addition, realistic simulation of the process of pollen pollination would make the algorithm particularly complex, which not only required a large amount of computing resources, but also led to low computational efficiency of the algorithm and little practical application value. To make the algorithm simple and easy, the flower pollination algorithm simulated the process of flower pollination in nature. FPA regulated the conversion between global search and local search by probability constant, and the value range of probability constant was 0–1. The specific mathematical implementation process of FPA algorithm was as follows:

(1) The mathematical definition of global search was $x_i^{t+1} = x_i^t + \gamma L(\lambda)\left(g_{\text{best}} - x_i^t\right)$, where x_i^t was the position of pollen when the current iteration number was t; g_{best} was the best position obtained under the current iteration; γ was the step size control parameter; $L(\lambda)$ was the flower pollination intensity, and $L(\lambda) > 0$;

(2) The mathematical definition of local search was $x_i^{t+1} = x_i^t + \varepsilon\left(x_j^t - x_k^t\right)$, where ε was the independent uniform distribution on [0, 1]; x_j^t and x_k^t was the different individuals from the same population, i.e., the same species of origin and different flowers.

2.3. Cross Validation and Model Performance Indicators

Cross validation was a statistical method to evaluate generalization performance. In the process of cross validation, the data were divided into K-folds, and each fold was employed as the test set in the training model, and other K-1 folds were employed as the training set. Finally, k precision values were obtained. A common method to evaluate the accuracy of cross validation was to calculate the average value, which made all categories of data able to be trained through K-fold division so that the model was more stable and the data were more comprehensive. Therefore, this work adopted K-fold cross validation to verify the accuracy and robustness of the machine learning model. Based on the above flower pollination algorithm, this work proposed a method which combined K-fold cross validation and flower pollination algorithm to optimize the model parameters of BP and ELM models. As shown in Figure 5, the basic connotation and implementation methods of FPA algorithm were as follows:

(1) Parameter initialization. Suppose the training sample was $[x_i, y_i](x_i \in \mathrm{R_n}$, n is the number of input neurons of the extreme learning machine model, I = 1,2 ... N, N is the total number of samples), constructed the excitation function of the extreme learning machine and set the number of nodes in the hidden layer, where C is the number of nodes in the hidden layer, g is the iteration times of the extreme learning machine model;

(2) Construct the fitness function of the extreme learning machine model. Taking the root-mean-square error of K-CV as the fitness of the extreme learning machine model, the individual with the smallest average RMSE was found;

(3) Iterative update. Calculate the fitness of the extreme learning machine model and update the individual accordingly;

(4) Optimal parameter generation of extreme learning machine model. Judge whether the preset algorithm termination requirements are met. If so, the optimal parameter combination of the extreme learning machine model is obtained. Otherwise, go back to step 2.

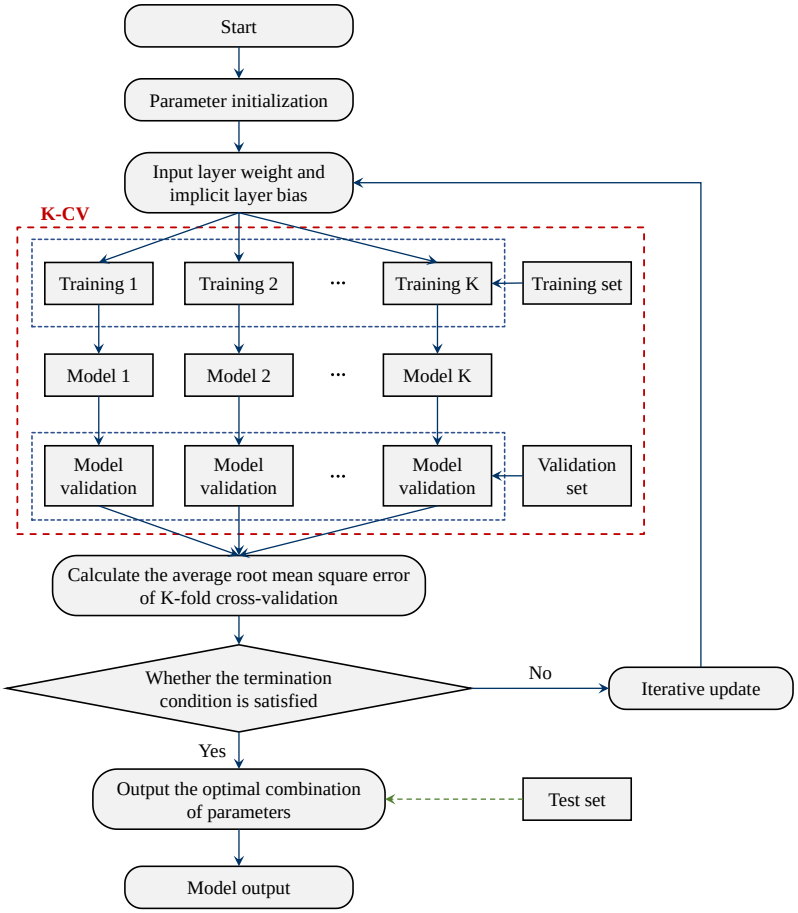

Figure 5. Schematic diagram of the implementation process of the fusion of K-CV and machine learning algorithm.

In this work, the FPA population size was set to 100, the maximum number of iterations was set to 1000, the constant P was set to 0.9, γ was set to 1, the average RMSE of K-CV was used as fitness function, and the activation function of the ELM model was selected as "sigmoid" function. Five-sixths of the sample data were selected as the training set, and the remaining one-sixth of the sample data were selected as the verification set.

The reliability and accuracy of the hybrid machine learning models were assessed using two evaluation indicators objectively, including the squared correlation coefficient R and RMSE. Their definitions were as follows:

$$R = \frac{\sum_{i=1}^{n}\left(\hat{Y}_i - \overline{\hat{Y}}\right)\left(Y_i - \overline{Y}\right)}{\sqrt{\sum_{i=1}^{n}\left(\hat{Y}_i - \overline{\hat{Y}}\right)^2}\sqrt{\sum_{i=1}^{n}\left(Y_i - \overline{Y}\right)^2}} \tag{7}$$

$$RMSE = \sqrt{\sum_{i=1}^{n}\left(Y_i - \hat{Y}_i\right)^2 / n} \tag{8}$$

where Y_i was the real value of oxide scale thickness, $\hat{Y}_i$ was the predicted value of oxide scale thickness estimated by machine learning model.

3. Results and Discussion

3.1. Microstructure and Mechanical Properties

There were 72 sample combinations under different process parameter combinations, which could not all be shown here. Typical samples were sampled and displayed to

reflect the general variation law of coating microstructure characteristics and mechanical properties under different process parameter combinations. As shown in Figure 6, the variation of porosity at different spraying distances prepared by coarse powder at 36 kW increased with the increase of spraying distance.

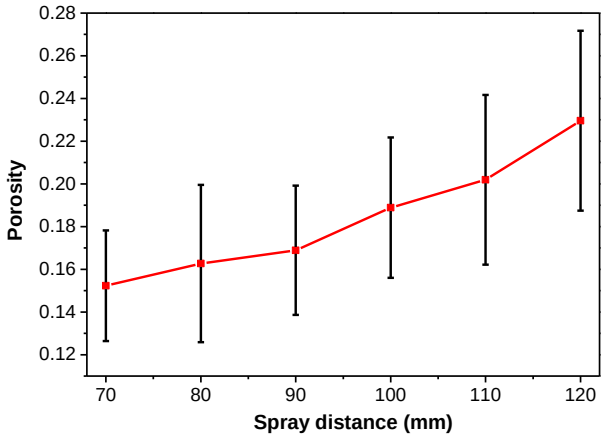

Figure 6. Porosity at different spray distances.

As shown in Figure 7, the circularity with different spraying distances prepared by coarse powder at 36 kW increased with the increase of spraying distance in the low value area of circularity. However, in the area where the value of circularity increased to almost 1, it tended to decrease.

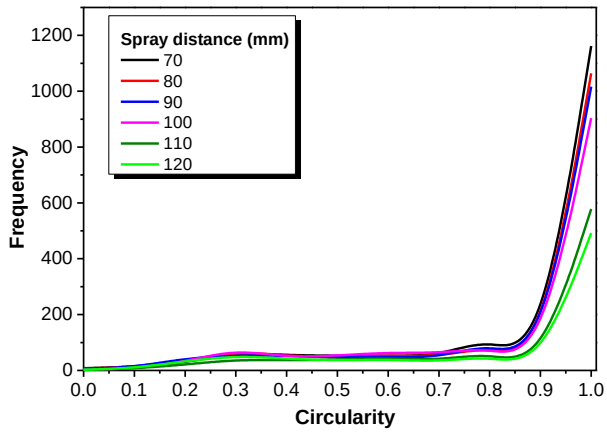

Figure 7. Circularity at different spray distances.

As shown in Figure 8, with the increase of spraying power, the distribution of Feret's diameter with different spraying power prepared by coarse powder at the spraying distance of 100 mm decreased in the low value area, but increased in the area that was enlarged.

As shown in Figure 9, the adhesive strength prepared by coarse powder at the spraying distance of 100 mm with different spraying powers increased with the increase of spraying power.

As shown in Figure 10, the hardness with different spraying power prepared by coarse powder at the spraying distance of 100 mm increased with the increase of spraying power.

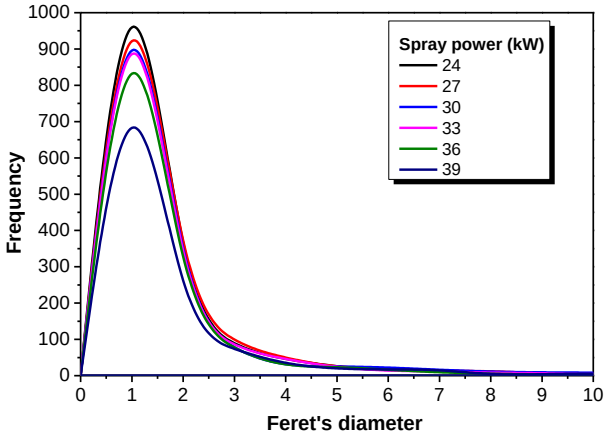

Figure 8. Feret's diameter at different spray powers.

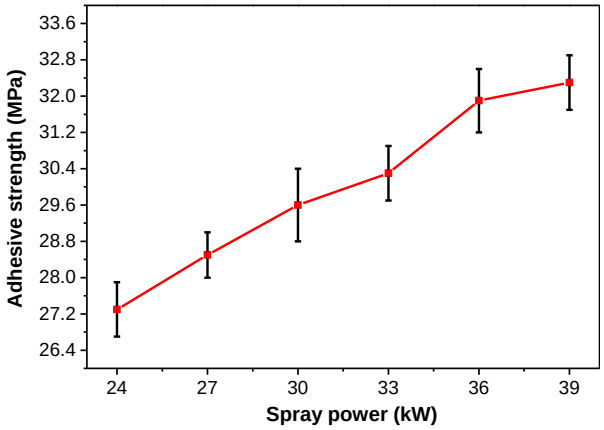

Figure 9. Adhesive strength at different spray powers.

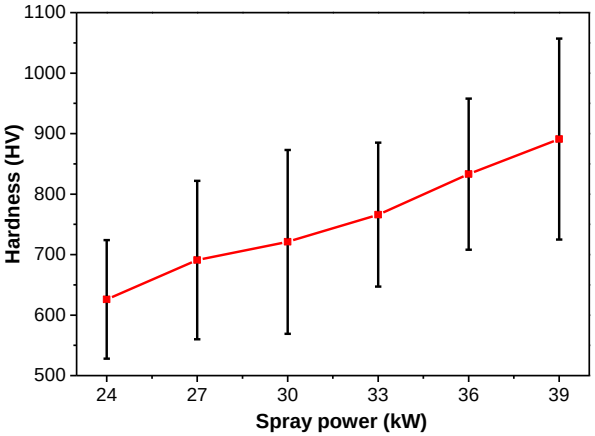

Figure 10. Hardness at different spray powers.

The above three microstructure parameters and two mechanical property parameters were only part of the structure and property parameters of TBCs. Previous relevant research studies also involved the research of related content. For atmospheric plasma TBCs, the failure standard of TBCs were the cracking and shedding. The greater the bonding strength of the interface between substrate and TBCs, the less easy it would be for the TBCs to fall off the substrate. Therefore, bonding strength and hardness were important mechanical properties to evaluate the performance of TBCs. For example, in the test range of this work, the binding strength increased with the increase of spraying power, and with the increase of

spraying power, the melting degree of powder particles was higher, powder droplets could be fully expanded during deposition, defects such as pores and voids inside the coating was reduced, and the binding strength was improved. Meanwhile, with the increase of spraying power, the plasma flame flow temperature increased, and then the temperature of the substrate subsequently increased, resulting in a certain heat-affected zone on the surface of the substrate. While the melt droplets were deposited in the heat-affected zone, there was a certain metallurgical bonding with the substrate, and the binding force was greater than the traditional mechanical bonding, so as to improve the bonding strength between the TBCs and the substrate.

The change of spraying process parameters would lead to the change of microstructure characteristics and mechanical properties. The atmospheric plasma spraying TBCs contained a large number of lamellar unbonded defects, macropores, vertical cracks and lamellar particle surfaces. The stacking mode of interlayer interfaces may affect the bonding strength of lamellar interfaces, and thus affecting the cracking resistance of the TBCs. The melting index of coating powder would be directly affected with the change of spraying process parameters, which would lead to the change of micro-pore structure parameters. Meanwhile, the mechanical properties of TBCs were affected by the change of microstructure characteristics. Therefore, the reduction of pores and cracks increased the density of TBCs, thus improving the hardness and the binding strength.

Many studies had shown that changes in micropore characteristics and mechanical properties of thermal barrier coatings caused by changes in process parameters were more of a qualitative or semi-quantitative characterization, which could not be directly employed to guide the quantitative preparation of coatings. Therefore, it would be fuzzy to regulate the microstructure of TBCs through changes in process parameters so as to improve their comprehensive properties, including the thermodynamic properties of TBCs. Therefore, the establishment of machine learning regression models, including spraying process parameters, microstructure parameters and mechanical properties, would be of great benefit to improve the service performance of TBCs.

3.2. Comparison of Various Prediction Models

As shown in Figure 11, the FPA-ELM model was trained through the training set composed of the microstructure and mechanical property data of 72 groups of thermal barrier coating test samples. The figure showed the fitness function change curve of porosity model training. It could be seen from the fitness evolution curve that while the training model was iterated for 386 times, the training error of FPA-ELM model parameters reached the minimum value and met the training requirements. In this case, it was considered that the optimal value could be obtained by reaching the critical maximum number of iterations.

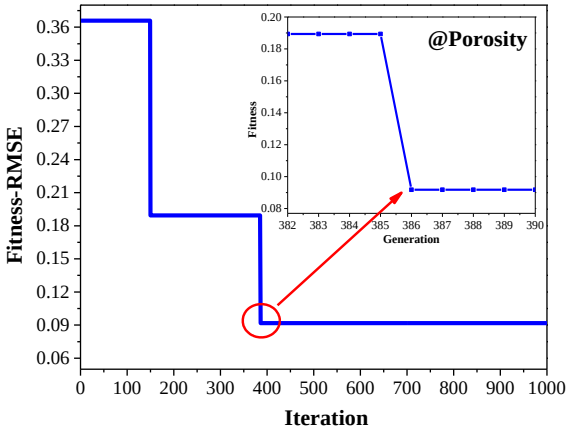

Figure 11. Fitness (RMSE) evolution curve of the porosity.

As shown in Figure 12, to further verify the prediction accuracy and robustness of the proposed machine learning model, K-fold cross validation was used to verify the model again [31]. Considering that the total number of sample data were 72, it was divided into 6 groups and verified for 6 times, respectively, so the design was a 6-fold cross validation.

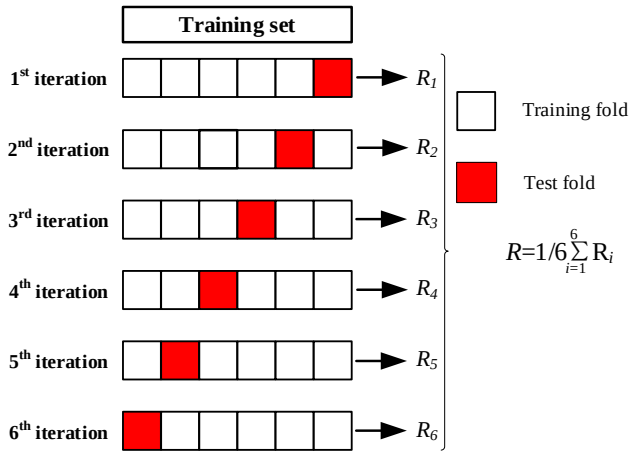

Figure 12. Schematic diagram of the 6-fold cross-validation process.

As shown in Table 1, from the perspective of *R*, the prediction results of the four models of BP, FPA-BP, ELM and FPA-ELM on the five parameters of thermal barrier coatings could be compared and analyzed. The conclusion could be drawn that the prediction performance of BP model without FPA optimization was unstable and had overall deviation compared with that of ELM model without FPA optimization. Although the regression prediction effect of the direct use of ELM model was improved compared with that of BP model, nevertheless, the overall prediction effect was still unsatisfactory.

Table 1. The R prediction comparison results of the five parameters of the BP, FPA-BP, ELM and FPA-ELM model.

Performance Indicator R	Porosity	Circularity	Feret's Diameter	Adhesive Strength	Hardness
BP	0.8219	0.7691	0.6219	0.6895	0.6021
FPA-BP	0.9437	0.9705	0.9413	0.9612	0.9426
ELM	0.9563	0.8033	0.7642	0.8003	0.8369
FPA-ELM	0.9715	0.9581	0.9503	0.9578	0.9709

As shown in the comparison between Tables 1 and 2, the following conclusions could be drawn when the four models of BP, FPA-BP, ELM and FPA-ELM were cross-verified by the 6-fold method: the predictive performance of the BP model without FPA optimization decreased rapidly and remained at a very low level. Compared with the BP model without FPA optimization, although the regression performance of the ELM model without FPA optimization was superior to that of the BP model without FPA optimization, it still could not meet the actual demand of regression prediction. At this time, it could be seen that after adding FPA optimization, the regression prediction effect of FPA-BP and FPA-ELM models had been greatly improved, in which the R-value of FPA-BP model was maintained at about 0.9, and the R-value of FPA-ELM model was over 0.94, indicating that the FPA-ELM model was comprehensively superior to FPA-BP model. It had better prediction accuracy and stability.

Table 2. The R prediction comparison results of the five parameters of the BP, FPA-BP, ELM and FPA-ELM model obtained by 6-fold CV.

Performance Indicator R K-CV	Porosity	Circularity	Feret's Diameter	Adhesive Strength	Hardness
BP	0.0952	0.2176	0.1846	0.2978	0.1763
FPA-BP	0.8935	0.9006	0.9003	0.8974	0.8996
ELM	0.4185	0.5127	0.4876	0.5189	0.6001
FPA-ELM	0.9411	0.9628	0.9788	0.9473	0.9516

Similar to the above analysis, as shown in Tables 3 and 4, from the perspective of RMSE, the prediction results of the four models of BP, FPA-BP, ELM and FPA-ELM on the five parameters of thermal barrier coating were compared and analyzed. For the five parameters, the RMSE values of the two regression models after FPA were maintained at a low level in their respective fields. In particular, the RMSE of the FPA-ELM model was below 1 on the remaining four characteristic parameters; however, hardness reached 1.9743. Therefore, by comparing and analyzing the regression effects of different prediction models, the above conclusions based on R-value analysis could be drawn, but not as high as the differentiation degree of R. However, it was still clear that FPA-ELM model was comprehensively superior to FPA-BP model, and FPA-ELM model had better pre-accuracy and stability.

Table 3. The RMSE prediction comparison results of the five parameters of the BP, FPA-BP, ELM and FPA-ELM model.

Performance Indicator RMSE	Porosity	Circularity	Feret's Diameter	Adhesive Strength	Hardness
BP	0.8536	1.0623	2.126	3.7415	24.1579
FPA-BP	0.3215	0.2215	1.0126	1.5768	4.7859
ELM	0.6547	0.9578	3.1245	2.1748	9.5762
FPA-ELM	0.2148	0.0954	0.1268	0.4785	2.9872

Table 4. The RMSE prediction comparison results of the five parameters of the BP, FPA-BP, ELM and FPA-ELM model obtained by 6-fold CV.

Performance Indicator RMSE K-CV	Porosity	Circularity	Feret's Diameter	Adhesive Strength	Hardness
BP	3.1458	1.8412	3.6547	3.0145	28.1144
FPA-BP	0.3254	0.3369	0.9142	1.8742	5.8423
ELM	0.5476	1.3247	4.6987	4.1785	7.3719
FPA-ELM	0.0917	0.1081	0.3697	0.2357	1.9743

In conclusion, it could be proven that the FPA-ELM model proposed in this study has good robustness and high reliability, and can provide artificial intelligence and big data methods to solve problems in the future in the study and characterization of the relationship between the preparation process parameters of thermal barrier coating, microstructure characteristics and mechanical properties.

4. Conclusions

In this work, it was shown that the spray process parameter had vital effects on the microstructure features and mechanical properties of the atmospheric plasma-sprayed YSZ coatings. Moreover, they had a complex nonlinear relationship and influenced each

other, and directly determined the service performance and life of TBCs. Through the combination of machine learning algorithm and intelligent optimization algorithm, it tried to solve the practical application problems that had puzzled the TBCs engineers for a long time. The obtained hybrid machine learning regression prediction model would be employed to achieve the quantitative control during TBCs preparation. Based on the above studies, the following conclusions could be made:

1. With the change of the spraying process parameters, the melting index in the deposition process would be directly affected, thus leading to the change of a variety of microstructural characteristic parameters, including porosity, circularity and Feret's diameter, which would directly affect the internal and interfacial mechanical properties. The coupling correlation between process parameters, microstructure parameters and mechanical properties, and direct exhaustive experiments for qualitative and semi-quantitative characterization were limited in guiding effect, so it was necessary and useful to combine big data technology to conduct quantitative modeling in a limited sample space;

2. According to the comparison of BP model and ELM model, it was found that the regression performance of ELM model was better than that of BP model. However, after the cross validation of k-fold, the optimization algorithm needed to be introduced to update the weights and thresholds iteratively to further improve the robustness and accuracy of the prediction model;

3. Finally, a hybrid machine learning regression prediction model named FPA-ELM was obtained, which showed relatively strong prediction and generalization ability after repeated training and verification. From this, we could make further prospects that machine learning would be expected to offer novel methods for the research and development of new TBCs materials, structural regulation and performance improvement through more data accumulation and in-depth training in the future.

Author Contributions: Conceptualization, H.Z.; Data curation, H.Z. and D.L.; Formal analysis, D.L.; Funding acquisition, D.Y.; Investigation, H.Z. and M.Y.; Methodology, D.Y.; Project administration, D.Y.; Resources, D.Y.; Software, H.Z. and D.L.; Supervision, D.Y.; Validation, H.Z. and M.Y.; Writing—original draft, H.Z.; Writing—review and editing, D.Y. All authors have read and agreed to the published version of the manuscript.

Funding: This work is supported by the Key Research and Development Projects in Anhui Province (2022a05020004), Open Research Fund of Anhui Key Laboratory of Mine Intelligent Equipment and Technology (ZKSYS202201), Open Research Fund of AnHui Key Laboratory of Detection Technology and Energy Saving Devices (JCKJ2022A08), Anhui Institute of Future Technology Enterprise Cooperation Project (2023qyhz04), Science and Technology Plan Project of Wuhu City (2022yf67, 2022jc48), Opening Project of Automotive New Technique of Anhui Province Engineering Technology Research Center (QCKJ202209B), National College Student Innovation and Entrepreneurship Training Program Project (202210363020).

Institutional Review Board Statement: Not applicable.

Informed Consent Statement: Not applicable.

Data Availability Statement: Not applicable.

Conflicts of Interest: The authors declare no conflict of interest.

References

1. Liu, J.; Lv, Z.; Zhou, Y.; Huang, S.; Chen, H.; Xu, N. Research progress of advanced ceramic materials for thermal barrier coatings. *Surf. Technol.* **2022**, *51*, 42–52.
2. Padture, N.P.; Gell, M.; Jordan, E.H. Thermal barrier coatings for gas-turbine engine applications. *Science* **2002**, *296*, 280–284. [CrossRef]
3. Gizynski, M.; Chen, X.; Dusautoy, N.; Araki, H.; Kuroda, S.; Watanabe, M.; Pakiela, Z. Comparative study of the failure mechanism of atmospheric and suspension plasma sprayed thermal barrier coatings. *Surf. Coat. Technol.* **2019**, *370*, 163–176. [CrossRef]
4. Yang, P.; Yue, W.; Li, J.; Bin, G.; Li, C. Review of damage mechanism and protection of aero-engine blades based on impact properties. *Eng. Fail. Anal.* **2022**, *140*, 106570. [CrossRef]
5. Lashmi, P.G.; Ananthapadmanabhan, P.V.; Unnikrishnan, G.; Aruna, S.T. Present status and future prospects of plasma sprayed multilayered thermal barrier coating systems. *J. Eur. Ceram. Soc.* **2020**, *40*, 2731–2745. [CrossRef]

6. Qiao, L.; Wu, Y.; Hong, S.; Cheng, J.; Wei, Z. Influence of the High-Velocity Oxygen-Fuel Spray Parameters on the Porosity and Corrosion Resistance of Iron-Based Amorphous Coatings. *Surf. Coat. Technol.* **2019**, *366*, 296–302. [CrossRef]
7. Balan, K.; Manimaran, S.; Rajan, A.J. Prediction of Interactions between Various Input Process Parameters Involved in Detonation Gun Coating Technique through Response Surface Methodology. *Proc. Eng.* **2014**, *97*, 1399–1405. [CrossRef]
8. Kamnis, S.; Malamousi, K.; Marrs, A.; Allcock, B.; Delibasis, K. Aeroacoustics and Artificial Neural Network Modeling of Airborne Acoustic Emissions during High Kinetic Energy Thermal Spraying. *J. Therm. Spray Technol.* **2019**, *28*, 946–962. [CrossRef]
9. Mahade, S.; Venkat, A.; Curry, N.; Leitner, M.; Joshi, S. Erosion Performance of Atmospheric Plasma Sprayed Thermal Barrier Coatings with Diverse Porosity Levels. *Coatings* **2021**, *11*, 21. [CrossRef]
10. Lima, R.S. Porous APS YSZ TBC Manufactured at High Powder Feed Rate (100 g/min) and Deposition Efficiency (70%): Microstructure, Bond Strength and Thermal Gradients. *J. Therm. Spray Technol.* **2022**, *31*, 396–414. [CrossRef]
11. Rejda, E.F.; Socie, D.F.; Beardsley, B. Fatigue behavior of a plasma-sprayed 8%Y_2O_3-ZrO_2 thermal barrier coating. *Fatigue Fract. Eng. Mater. Struct.* **2010**, *20*, 1043–1050. [CrossRef]
12. Wang, J.; Bai, L.; Ma, F.; Wan, S.; Yi, G.; Sun, J.; Tian, X.; Yang, Z. Evaluation of microstructure evolution of thermal barrier YSZ coating after thermal exposure. *Ceram. Int.* **2022**, *48*, 6681–6690. [CrossRef]
13. Giyński, M.; Chen, X.; Araki, H.; Tanaka, H.; Kuroda, S.; Watanabe, M.; Pakieła, Z. Sintering Characteristics of Thermal Barrier YSZ Coatings Made by Suspension Plasma Spraying. *J. Therm. Spray Technol.* **2022**, *31*, 1521–1539. [CrossRef]
14. Roncallo, G.; Barbareschi, E.; Cacciamani, G.; Vacchieri, E. Effect of cooling rate on phase transformation in 6–8 wt% YSZ APS TBCs. *Surf. Coat. Technol.* **2021**, *412*, 127071. [CrossRef]
15. Edward, J.; Sampath, S. Durability of Plasma Sprayed Thermal Barrier Coatings with Controlled Properties Part I: For Planar Disk Substrates. *Surf. Coat. Technol.* **2021**, *424*, 127678.
16. Tillmann, W.; Khalil, O.; Baumann, I. Influence of Direct Splat-Affecting Parameters on the Splat-Type Distribution, Porosity, and Density of Segmentation Cracks in Plasma-Sprayed YSZ Coatings. *J. Therm. Spray Technol.* **2021**, *30*, 1015–1027. [CrossRef]
17. Saremi, M.; Valefi, Z. The effects of spray parameters on the microstructure and thermal stability of thermal barrier coatings formed by solution precursor flame spray (spfs). *Surf. Coat. Technol.* **2013**, *220*, 44–51. [CrossRef]
18. Karabaş, M.; Bal, E.; Kilic, A.; Taptık, İ.Y. Effect of Air Plasma Spray Parameters on the Properties of YSZ and CYSZ Thermal Barrier Coatings. *J. Australas. Ceram. Soc.* **2016**, *52*, 175–182.
19. Arhami, F.; Ben Ettouil, F.; Moreau, C. As-Sprayed Highly Crystalline $Yb_2Si_2O_7$ Environmental Barrier Coatings (EBCs) by Atmospheric Plasma Spray (APS). *J. Therm. Spray Technol.* **2023**, 1–13. [CrossRef]
20. Vaen, R.; Bakan, E.; Mack, D.E.; Guillon, O. A Perspective on Thermally Sprayed Thermal Barrier Coatings: Current Status and Trends. *J. Therm. Spray Technol.* **2022**, *31*, 685–698.
21. Sobhanverdi, R.; Akbari, A. Porosity and microstructural features of plasma sprayed Yttria stabilized Zirconia thermal barrier coatings. *Ceram. Int.* **2015**, *41*, 14517–14528. [CrossRef]
22. Ye, D.; Wang, W.; Zhou, H.; Fang, H.; Huang, J.; Li, Y.; Gong, H.; Li, Z. Characterization of thermal barrier coatings microstructural features using terahertz spectroscopy. *Surf. Coat. Technol.* **2020**, *394*, 125836. [CrossRef]
23. Li, R.; Ye, D.; Xu, Z.; Yin, C.; Xu, H.; Zhou, H.; Yi, J.; Chen, Y.; Pan, J. Nondestructive Evaluation of Thermal Barrier Coatings Thickness Using Terahertz Time-Domain Spectroscopy Combined with Hybrid Machine Learning Approaches. *Coatings* **2022**, *12*, 1875. [CrossRef]
24. Shah, M.I.; Alaloul, W.S.; Alqahtani, A.; Aldrees, A.; Musarat, M.A.; Javed, M.F. Predictive Modeling Approach for Surface Water Quality: Development and Comparison of Machine Learning Models. *Sustainability* **2021**, *13*, 7515. [CrossRef]
25. Javed, M.F.; Farooq, F.; Memon, S.A.; Akbar, A.; Khan, M.A.; Aslam, F.; Alyousef, R.; Alabduljabbar, H.; Rehman, S.K.U. New Prediction Model for the Ultimate Axial Capacity of Concrete-Filled Steel Tubes: An Evolutionary Approach. *Crystals* **2020**, *10*, 741. [CrossRef]
26. Ye, D.; Xu, Z.; Pan, J.; Yin, C.; Hu, D.; Wu, Y.; Li, R.; Li, Z. Prediction and Analysis of the Grit Blasting Process on the Corrosion Resistance of Thermal Spray Coatings Using a Hybrid Artificial Neural Network. *Coatings* **2021**, *11*, 1274. [CrossRef]
27. Ye, D.; Wang, W.; Xu, Z.; Yin, C.; Zhou, H.; Li, Y. Prediction of Thermal Barrier Coatings Microstructural Features Based on Support Vector Machine Optimized by Cuckoo Search Algorithm. *Coatings* **2020**, *10*, 704. [CrossRef]
28. Xu, Z.; Ye, D.; Chen, J.; Zhou, H. Novel Terahertz Nondestructive Method for Measuring the Thickness of Thin Oxide Scale Using Different Hybrid Machine Learning Models. *Coatings* **2020**, *10*, 805. [CrossRef]
29. Shah, M.I.; Javed, M.F.; Aslam, F.; Alabduljabbar, H. Machine learning modeling integrating experimental analysis for predicting the properties of sugarcane bagasse ash concrete. *Constr. Build. Mater.* **2022**, *314*, 125634. [CrossRef]
30. Yang, X.S. Flower Pollination Algorithm for Global Optimization. In *Unconventional Computation and Natural Computation*; Durand-Lose, J., Jonoska, N., Eds.; UCNC 2012; Lecture Notes in Computer Science; Springer: Berlin/Heidelberg, Germany, 2012; Volume 7445. [CrossRef]
31. Jung, Y.; Hu, J. A *K*-fold averaging cross-validation procedure. *J. Nonparametric Stat.* **2015**, *27*, 167–179. [CrossRef]